Precision Chemoradiotherapy for HER2 Tumors Using Antibody Conjugates of an Auristatin Derivative with Reduced Cell Permeability

Dina V. Hingorani[1], Matthew K. Doan[1], Maria F. Camargo[1], Joseph Aguilera[1], Seung M. Song[2], Donald Pizzo[2], Daniel J. Scanderbeg[1], Ezra E.W. Cohen[3,4], Andrew M. Lowy[4,5], Stephen R. Adams[6], and Sunil J. Advani[1,4]

ABSTRACT

The most successful therapeutic strategies for locally advanced cancers continue to combine decades-old classical radiosensitizing chemotherapies with radiotherapy. Molecular targeted radiosensitizers offer the potential to improve the therapeutic ratio by increasing tumor-specific kill while minimizing drug delivery and toxicity to surrounding normal tissue. Auristatins are a potent class of anti-tubulins that sensitize cells to ionizing radiation damage and are chemically amenable to antibody conjugation. To achieve tumor-selective radiosensitization, we synthesized and tested anti-HER2 antibody–drug conjugates of two auristatin derivatives with ionizing radiation. Monomethyl auristatin E (MMAE) and monomethyl auristatin F (MMAF) were attached to the anti-HER2 antibodies trastuzumab and pertuzumab through a cleavable linker. While MMAE is cell permeable, MMAF has limited cell permeability as free drug resulting in diminished cytotoxicity and radiosensitization. However, when attached to trastuzumab or pertuzumab, MMAF was as efficacious as MMAE in blocking HER2-expressing tumor cells in G_2–M. Moreover, MMAF anti-HER2 conjugates selectively killed and radiosensitized HER2-rich tumor cells. Importantly, when conjugated to targeting antibody, MMAF had the advantage of decreased bystander and off-target effects compared with MMAE. In murine xenograft models, MMAF anti-HER2 antibody conjugates had less drug accumulated in the normal tissue surrounding tumors compared with MMAE. Therapeutically, systemically injected MMAF anti-HER2 conjugates combined with focal ionizing radiation increased tumor control and improved survival of mice with HER2-rich tumor xenografts. In summary, our results demonstrate the potential of cell-impermeable radiosensitizing warheads to improve the therapeutic ratio of radiotherapy by leveraging antibody–drug conjugate technology.

Introduction

Nonmetastatic, locally advanced cancers remain a therapeutic challenge to eradicate. Their infiltrative nature into surrounding critical normal structures precludes surgical resection. For such patients, combining chemotherapy and radiotherapy forms the basis of organ-sparing curative treatment (1–3). The paradigm of concurrent cytotoxic chemotherapy [i.e., cisplatinum, paclitaxel, 5-fluorouracil (5-FU), and mitomycin C] and radiotherapy was established over four decades ago (4). Subsequent randomized control trials across diverse tumor histologies have consistently demonstrated superior tumor control, organ preservation, and/or patient survival when radiotherapy is delivered with chemotherapy (4–10).

Although cytotoxic chemotherapies improve tumor control with radiotherapy, these nontargeted drugs increase normal tissue damage in the irradiated field in addition to their systemic toxicities (1–3). Treatment-induced side effects during therapy interfere with delivering full-dose chemotherapy and radiotherapy resulting in treatment delays and/or dose reduction negatively affecting patient outcomes. Moreover, long-term normal tissue collateral damage diminishes patient quality of life. Finally, dose-limiting toxicities preclude further treatment intensification to improve cancer cure. For these reasons, more targeted means of achieving tumor radiosensitization are needed (1, 2, 11–14). Elucidating the molecular underpinnings of cellular responses to ionizing radiation (IR) and DNA damage have identified druggable targets to improve IR kill. Unfortunately, clinical success with inhibitors of DNA damage repair is lacking (15–17). One explanation for the lack of progress beyond current chemoradiotherapy regimens is that conventional cytotoxic chemotherapies set a high bar that more targeted radiosensitizing drugs have difficulty surpassing because in addition to any radiosensitization potential, cisplatin, taxanes, and 5-FU have an established role in cancer therapy for their intrinsic tumoricidal activity (3).

An alternative strategy to improve the chemoradiotherapy paradigm is using cytotoxins more potent than standard chemotherapies with the caveat of restricting drug delivery to tumors and limiting normal tissue damage both in and out of the irradiated field by leveraging antibody–drug conjugate (ADC) technology (18–20). ADCs split the roles of tumor targeting and cell killing into two distinct molecular tasks. Targeting is achieved by antibodies recognizing cell surface receptors preferentially expressed on tumor cells.

[1]Department of Radiation Medicine and Applied Sciences, University of California San Diego, La Jolla, California. [2]Department of Pathology, University of California San Diego, La Jolla, California. [3]Division of Hematology and Oncology, Department of Medicine, University of California San Diego, La Jolla, California. [4]University of California San Diego, Moores Cancer Center, La Jolla, California. [5]Division of Surgical Oncology, Department of Surgery, University of California San Diego, La Jolla, California. [6]Department of Pharmacology, University of California San Diego, La Jolla, California.

Note: Supplementary data for this article are available at Molecular Cancer Therapeutics Online (http://mct.aacrjournals.org/).

D.V. Hingorani and M.K. Doan contributed equally to this article.

Corresponding Author: Sunil J. Advani, University of California San Diego, 3855 Health Sciences Drive, MC #0843, La Jolla, CA 92093-0843. Phone: 858-822-6046; Fax: 858-822-5568; E-mail: sjadvani@ucsd.edu

Mol Cancer Ther 2020;19:157–67

doi: 10.1158/1535-7163.MCT-18-1302

Tumor kill is mediated by the release of attached drug payload, that is, warhead. Following receptor-mediated binding of the antibody, the warhead is specifically delivered to target-enriched tumors. Patient safety and efficacy have been established with at least five ADCs, brentuximab vedotin (Adcetris, Seattle Genetics), T-DM1 (Kadcyla, Roche-Genentech), inotuzumab ozogamicin (Besponsa, Pfizer), gemtuzumab ozogamicin (Mylotarg, Pfizer), and polatuzumab vedotin (Polivy, Roche-Seattle Genetics; refs. 21–28).

The monomethyl auristatin E (MMAE) and mertansine warheads for three of these clinically approved ADC (brentuximab vedotin, polatuzumab vedotin, and T-DM1) are anti-tubulins that can radiosensitize (29–31). However, both of these anti-tubulins are cell permeable as free drug. Release of cell-permeable warheads from ADCs in the context of concurrent radiotherapy raises concerns of bystander toxicity and surrounding normal tissue radiosensitization. This would negate the therapeutic gain of ADC-guided drug delivery with IR. An indirect solution to this problem uses a noncleavable linker (i.e., T-DM1), where lysosomal processing results in a slow release of a lysine conjugated to mertansine via a noncleavable thioether linker producing a diffusion-restricted drug (32). However, release of noncleavable linkers from lysosomes is slow, and trafficking regulators influence ADC toxicity (33, 34). A more direct strategy to decrease off-target bystander toxicity is to use radiosensitizing warheads that are intrinsically less cell permeable when released from the targeting antibody. MMAE belongs to a family of auristatin derivatives that block cells in the radiosensitive G_2–M phase of the cell cycle. Although MMAE freely diffuses into cells, the monomethyl auristatin F (MMAF) derivative has decreased cell permeability as a free drug resulting in reduced cytotoxicity (35, 36). Importantly, MMAF can be coupled to targeting antibodies via a cleavable linker that is efficiently processed within endolysosomes to maintain receptor-restricted tumor kill.

To improve the therapeutic ratio of auristatin ADCs in the context of localized cancers treated with radiotherapy, we synthesized anti-HER2 antibody conjugates of MMAF and tested them with IR. MMAF attached to anti-HER2 antibodies pertuzumab (P-MMAF) or trastuzumab (T-MMAF) blocked cells in G_2–M resulting in cell kill and radiosensitization of HER2-expressing cells *in vitro*. When directly compared with MMAE, antibody-conjugated MMAF had decreased bystander cytotoxicity in cell culture. Advancing to murine tumor xenograft models, intravenously injected Cy5-labeled P-MMAF and T-MMAF spatially localized to HER2-overexpressing tumors. Importantly, MMAF antibody conjugates had lower drug accumulation in the normal tissue surrounding HER2-positive tumors compared with MMAE. Finally, MMAF anti-HER2 antibody conjugates combined with IR increased tumor control and mouse survival. In summary, our data demonstrate antibody conjugates of a nonpermeable auristatin variant are tumoricidal and radiosensitizing while reducing bystander toxicity and have translational potential for improving the chemoradiotherapy paradigm.

Materials and Methods

Cells and reagents

HCT116 colorectal and NCI N87 gastric cancer cell lines were obtained and authenticated by the ATCC. Esophageal cancer cell line OE19 was obtained from Sigma-Aldrich and authenticated by European Collection of Authenticated Cell Cultures (ECACC). HCT116 cells were cultured in DMEM supplemented with 10% FBS. OE19 and NCI N87 cells were cultured in RPMI supplemented with 10% FBS. On initial receipt, cell lines were expanded and low-passage stocks cryopreserved without further authentication testing. Cells were passaged 2 times per week and used for 4 to 6 weeks after which a new stock vial was thawed. Cells were routinely tested for *Mycoplasma* by PCR, and testing was performed prior to cell implantation in mice for xenograft experiments. Cell line HER2 status was tested by immunoblotting. MMAE and MMAF (Levena Biopharma) were reconstituted in DMSO. Clinical-grade trastuzumab and pertuzumab were obtained from UCSD Moores Cancer Center pharmacy.

Synthesis of Cy5-labeled anti-HER2 antibody conjugates of MMAE and MMAF

Pertuzumab and trastuzumab MMAF and MMAE conjugates were synthesized using established methods (37, 38). Specifically, a solution (1 mL, 2 mg/mL) of pertuzumab (Perjeta, Roche) or trastuzumab (Herceptin, Roche) was treated with sodium bicine buffer (100 μL, 1 mol/L, pH 8.3) and sodium diethylenetriaminepentaacetic acid (10 μL, 100 mmol/L, pH 7). Following reduction with 4 equivalents of tris (carboxyethyl)phosphine (TCEP) at 37°C for 2 hours, the solution was added to four equivalents of maleimidocaproyl-valine-citrulline-PABA-MMAE (MC-VC-MMAE, Levena Biopharma) or maleimidocaproyl-valine-citrulline-PABA-MMAF (MC-VC-MMAF, Levena Biopharma; refs. 39, 40). After 30 minutes at room temperature, Cy5-maleimide (two equivalents) was added and after 30 minutes, gel-filtered (Sephadex G25, 0.6 g) eluting with PBS. Following centrifugal concentration (Centricon 30 kDa MWCO) to 500 μL, concentration of antibody and Cy5 was determined by absorbance using extinction coefficients of 225,000 L/mol/cm (antibody) at 280 nm and 12,500 $M^{-1}cm^{-1}$ and 250,000 L/mol/cm at 280 nm and 650 nm, respectively, for Cy5. Hydrophobic interaction chromatography after labeling with MMAE or MMAF revealed 9 peaks corresponding to antibody modified with 0 to 8 MMAE or MMAF derivatives if up to 4 disulfides are reduced by TCEP per antibody (Supplementary Fig. S1). Subsequent Cy5-maleimide labeling gave 650 nm absorbance to each peak apart from that labeled with 8 MMAE or 8 MMAF as no cysteines are available for further conjugation (Supplementary Fig. S1). Drug loading was measured by denaturing reverse-phase high-performance liquid chromatography (HPLC) of the reaction mix prior to adding Cy5 maleimide. Peaks corresponding to light or heavy chains with 0 to 3 MMAE or MMAF were identified by electrospray mass spectroscopy (Supplementary Fig. S1), and peak areas at 280 nm were integrated and weighted to calculate drug loading. Modified light chain (L1) and unmodified H chain (H0) were not resolved for trastuzumab so MMAE loading is underestimated. No free MC-VC-MMAE or MC-VC-MMAF were detected by HPLC following gel filtration (41).

ADC cell binding

For Cy5 imaging, cells were exposed to Cy5-labeled P-MMAF or T-MMAF for 30 minutes in media with 1% serum. Cells were then washed with PBS and incubated in media with 10% serum. At 2 hours, cells were fixed in 4% paraformaldehyde, stained with DAPI, and imaged using a Nikon A1R confocal microscope for Cy5 and DAPI signal. For ADC cell surface binding, cells were resuspended in cold PBS with 1% BSA. Cy5-labeled pertuzumab-MMAE (P-MMAE), P-MMAF, trastuzumab-MMAE (T-MMAE), or T-MMAF was added to the cells for 30 minutes on ice. Cells were washed, resuspended in PBS with 1% BSA and 1 μg/mL DAPI, and analyzed by flow cytometry for Cy5. The *y* axis is reported as a percentage of maximum where each peak has been normalized to the peak height at its mode of distribution resulting in each peak with a maximum set at 100%. Data were analyzed using FlowJo software as described in the Univariate Display Comparison section of the software manual.

Cell cycle

Cells were drug treated for 24 hours, fixed in 70% ethanol, treated with FxCyclePI/RNase staining solution (Life Technologies), and then analyzed by FACS using FlowJo software.

Alamar Blue assay

Cells were plated in 96-well plates and exposed to a drug concentration range for 72 hours. Alamar Blue was added to the cells and allowed to incubate for 4 to 8 hours at 37°C. Plates were analyzed using a plate reader with fluorescence measured at 560 nm. Cell survival was normalized to untreated cells. For bystander cytotoxicity assays, conditioned media were collected from drug-treated host cells after 48 hours. Target cells were then exposed to conditioned media for 72 hours and analyzed by Alamar Blue.

Neutral comet assay

Cells were drug treated overnight and then irradiated with 2 Gy. Cells were harvested 20 minutes after IR, suspended in agarose gel, and lysed (Trevigen). Samples underwent electrophoresis in neutral conditions and stained with Sybr Green. Comet tails were measured in multiple independent fields and analyzed using CometScore (TriTek Corp). Comet tail length was normalized to nonirradiated cells.

Tumor drug measurement

All animal work was done in compliance with the University of California San Diego Institutional Animal Care and Use Committee (42). Six- to 8-week-old female athymic nu/nu mice from the University of California San Diego Animal Care Program were injected subcutaneously with 5 million HCT116, OE19, or NCI N87 cells in 100 μL of 1:1 Matrigel (BD Biosciences) and PBS solution. When tumors were palpable, mice were intravenously injected through the tail vein with 1 nmol of ADC in 50 μL of PBS. Tumors were excised on days indicated in figure legends, weighed, and homogenized in 10 v/w of 2% acetic acid in 1:1 acetonitrile: water with a point sonicator (Thermo Fisher Scientific) using an amplitude range of 5%–15% for 20 seconds on ice. Homogenates were centrifuged (14 × *g*, 10 minutes), and supernatants were collected for drug concentration measurements using LC/MS-MS. MMAE or MMAF concentration was determined by LC/MS-MS with Luna-2 C18 column and Agilent Trap XCT mass spectrometer. To determine MMAF tissue concentrations, ion currents for m/z 722.4 and 607.4 were extracted from fragmented m/z 754.5, and m/z 700.4 and 520.4 were extracted from fragmented m/z 732.5. Ion currents were integrated and combined to improve sensitivity. For MMAE tissue concentrations, integrated ion currents for m/z 682.4, 496.4 and m/z 686.4, 506.4 extracted from fragmented m/z 740.4 and 718.4, respectively, were combined. The total ion current was fit to a standard curve generated for each drug to quantitate tissue drug concentration.

IHC

When tumors were palpable, mice were intravenously injected through the tail vein with drug. Tumor and adjacent normal tissue muscle were excised at time points indicated in the Results and figure legends. Tissue was sectioned from formalin-fixed, paraffin-embedded blocks. Two adjacent 5 μm sections were cut and placed in the same slide. Sections were stained with antibody to phospho S10-histone H3 diluted 1:450 (Abcam; catalog no. ab32107) on a Ventana Discovery Ultra (Ventana Medical Systems). Antigen retrieval was performed using CC1 (tris-based; pH 8.5) for 24 minutes at 95°C. Primary antibody was incubated for 1 hour at 37°C. Secondary antibody (horseradish peroxidase–coupled goat anti-rabbit; UltraMap system; Ventana) was incubated for 12 minutes at 37°C. Primary antibody was visualized using DAB as a chromagen followed by hematoxylin counterstaining. Slides were rinsed, dehydrated through alcohol and xylene, and coverslipped. Serial sections were also hematoxylin and eosin (H&E) stained.

Slide scanning and immunostaining quantitation

Phospho S10-histone H3–stained slides were scanned using Axio Scan.Z1 and Zen2 software for automatic thresholding and tissue detection (Zeiss). The entire tissue section was scanned at 20X using default stitching parameters to merge individual tiles into a single image. Slide images were imported into Definiens Software for quantitative analysis using color contrast of the DAB and hematoxylin counterstain to identify regions of interest (ROI; Definiens). Software was trained to identify ROI. Total number of nuclei (hematoxylin-positive plus pS10 Histone H3-immunoreactive nuclei), stain intensity, stain area, and percent positive nuclei pS10 Histone H3/(pS10 Histone H3+hematoxylin) within the ROI based upon training were quantitated. Data were normalized to untreated control tumors.

In vivo tumor xenograft optical imaging

Tumor volume was measured with digital calipers using the formula $^1/_2 \times \text{Length} \times \text{Width}^2$. After tumors grew to approximately 200 mm^3 size, mice were intravenously injected through the tail vein with 1 nmol of drug in 50 μL water. Mice were anesthetized with isoflurane 24 hours after injection and whole animal Cy5 fluorescence visualized using a Xenogen IVIS 200 Imaging System. Cy5.5 excitation and emission filters were used with the following settings: 0.5-second exposure time, medium binning, lamp level high and filter lock. Fluorescence images were processed with Caliper Lifesciences Living Imaging software version 4.2.

In vivo tumor xenograft response experiments

Mice were randomized into treatment groups once mean tumor volumes reached >100 mm^3. Drug was intravenously injected through the tail vein in 50 μL. Following a single injection of ADC on day 0, tumors were irradiated with 2.5 Gy on days 1, 2, and 3. For irradiation, tumor-bearing hind limbs were focally irradiated with the remainder of the mouse shielded with custom lead blocking >95% of the IR dose as verified by dosimeters. To prevent unnecessary morbidity, mice were sacrificed if tumor length exceeded 15 mm. To minimize the number of mice used, tumors were grown in bilateral flanks. For NCI N87 tumor xenografts in **Fig. 5B**, the number of mice and tumors per group were: Control (5 mice, 10 tumors), P-MMAF (5 mice, 10 tumors), and T-MMAF (5 mice, 10 tumors). For NCI N87 tumor xenografts in **Fig. 5D**, the number of mice and tumors per group were: control (2 mice, four tumors), IR (3 mice, six tumors), T-MMAF (5 mice, 10 tumors), and T-MMAF+ IR (5 mice, 10 tumors). For OE19 tumor xenografts in **Fig. 5G**, the number of mice and tumors per group were: control (5 mice, 10 tumors), IR (5 mice, 10 tumors), pertuzumab (5 mice, 10 tumors), pertuzumab + IR (5 mice, 10 tumors), P-MMAF (5 mice, 10 tumors), and P-MMAF + IR (5 mice, 10 tumors).

Statistical analysis

Unpaired two-sided *t* tests or ANOVA with multiple comparisons were performed for cell culture experiments. For tumor regression studies, two-way ANOVA analysis was performed with Tukey multiple comparison group. Survival curves were analyzed by the Log-rank. All statistical analyses were performed using Prism software (GraphPad). Statistical analysis for tumor xenograft data are shown in Supplementary Table S1.

Results

Synthesizing MMAF anti-HER2 antibody conjugates

An advantage of auristatins is that they are highly potent cytotoxic drugs. Compared with conventional chemotherapies used with radiotherapy (i.e., paclitaxel and cisplatin) or a more specific EGFR/HER2 tyrosine kinase inhibitor (lapatinib), MMAE had a significantly lower IC_{50} in gastrointestinal cancer cell lines (**Fig. 1A**). To improve the therapeutic index of auristatin ADC when combined with IR, we evaluated MMAF which structurally differs from MMAE by having a charged phenylalanine on its C-terminus, impairing its cell membrane permeability (**Fig. 1B**; ref. 35). As a consequence of this modification, free MMAF has reduced potency compared with MMAE (**Fig. 1A**). Like MMAE, MMAF is chemically amenable to antibody conjugation. Therefore, we synthesized ADCs by conjugating MMAF to anti-HER2 antibodies pertuzumab and trastuzumab at endogenous cysteines by selective reduction of four disulfides in the antibody hinge region to create P-MMAF and T-MMAF, respectively (37, 39). To noninvasively track P-MMAF and T-MMAF, Cy5 was attached. On average, 4 MMAF and 1 Cy5 were conjugated per antibody (**Fig. 1C**). Similarly, MMAE was attached to pertuzumab and trastuzumab, P-MMAE and T-MMAE. Synthesized native ADCs were analyzed by hydrophobic interaction chromatograms and drug loading measured by denaturing reverse-phase protein chromograms with electrospray mass spectroscopy (Supplementary Fig. S1). To test binding of these synthesized pertuzumab and trastuzumab ADCs, we used gastrointestinal cancer cell lines differing in HER2 expression (**Fig. 1D**; Supplementary Fig. S2A). HER2-rich gastric NCI N87 and esophageal OE19 cell lines or HER2-negative colorectal HCT116 cell lines were incubated with

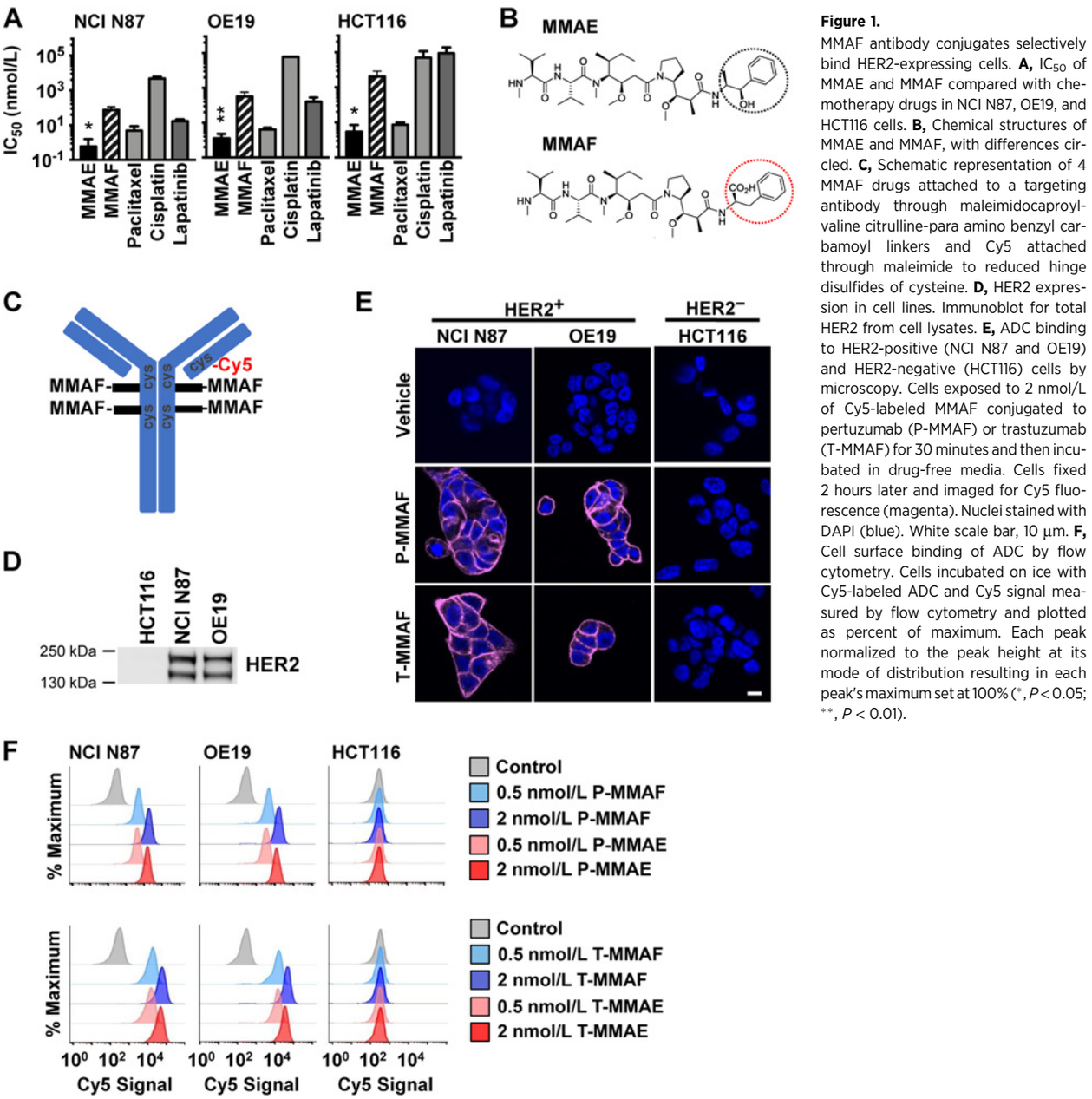

Figure 1.

MMAF antibody conjugates selectively bind HER2-expressing cells. **A,** IC_{50} of MMAE and MMAF compared with chemotherapy drugs in NCI N87, OE19, and HCT116 cells. **B,** Chemical structures of MMAE and MMAF, with differences circled. **C,** Schematic representation of 4 MMAF drugs attached to a targeting antibody through maleimidocaproyl-valine citrulline-para amino benzyl carbamoyl linkers and Cy5 attached through maleimide to reduced hinge disulfides of cysteine. **D,** HER2 expression in cell lines. Immunoblot for total HER2 from cell lysates. **E,** ADC binding to HER2-positive (NCI N87 and OE19) and HER2-negative (HCT116) cells by microscopy. Cells exposed to 2 nmol/L of Cy5-labeled MMAF conjugated to pertuzumab (P-MMAF) or trastuzumab (T-MMAF) for 30 minutes and then incubated in drug-free media. Cells fixed 2 hours later and imaged for Cy5 fluorescence (magenta). Nuclei stained with DAPI (blue). White scale bar, 10 μm. **F,** Cell surface binding of ADC by flow cytometry. Cells incubated on ice with Cy5-labeled ADC and Cy5 signal measured by flow cytometry and plotted as percent of maximum. Each peak normalized to the peak height at its mode of distribution resulting in each peak's maximum set at 100% (*, $P < 0.05$; **, $P < 0.01$).

Cy5-labeled P-MMAF and T-MMAF and fluorescence visualized (**Fig. 1E**; Supplementary Fig. S2B). Both P-MMAF and T-MMAF bound specifically to HER2-expressing cells. To validate these observations and test MMAF antibody conjugate binding compared with MMAE, cell surface–bound Cy5-labeled ADC was quantitated by flow cytometry (**Fig. 1F**). Both NCI N87 and OE19 cells exhibited dose-dependent cell surface binding of P-MMAF, P-MMAE, T-MMAF, and T-MMAE. The cell surface binding of pertuzumab or trastuzumab was independent of conjugated drug warhead, i.e., MMAE or MMAF. In contrast, HER2-negative HCT116 cells showed no shift in fluorescence signal when incubated with Cy5-labeled pertuzumab or trastuzumab auristatin conjugates.

Antibody conjugation is necessary for MMAF cytotoxicity and radiosensitization

We next evaluated the anti-tubulin functionality of auristatin warheads attached to pertuzumab or trastuzumab (**Fig. 2A**). Free MMAE resulted in all cell lines accumulating in G_2–M irrespective of HER2 status. However, pertuzumab or trastuzumab conjugation restricted MMAE G_2–M block to HER2-positive cells. Although free MMAF did not influence cell-cycle distribution, P-MMAF and T-MMAF both blocked NCI N87 and OE19 cells in G_2–M but had no effect on HER2-negative HCT116 cells. In contrast to the stark functional differences seen with free MMAE and MMAF, anti-HER2 antibody conjugates of both auristatin derivatives produced similar cell-cycle profiles in HER2-expressing cells. Next, we evaluated the potency of MMAF antibody conjugates (**Fig. 2B**). Cells were drug treated for 72 hours and viability measured. Consistent with the cell-cycle profiles, MMAE indiscriminately killed cancer cells with high potency irrespective of HER2 status, whereas free MMAF had significantly reduced potency. The IC_{50}s of free MMAE and MMAF were 0.7 and 88.3 nmol/L in NCI N87 cells, 1.5 and 386.3 nmol/L in OE19 cells N87, and 8.8 nmol/L and 8,944 nmol/L in HCT116 cells, respectively. Importantly, P-MMAF and T-MMAF conjugates had potencies comparable with free MMAE in HER2-expressing cell lines. The IC_{50} of P-MMAF and T-MMAF was 0.07 and 0.09 nmol/L in NCI N87 cells and 0.16 and 0.18 nmol/L in OE19 cells, respectively. In contrast, P-MMAF and T-MMAF were essentially nontoxic in HCT116 cells. Finally, we tested the ability of MMAF antibody conjugates to radiosensitize by increasing DNA double-strand breaks (**Fig. 2C**). Although MMAE significantly increased IR-induced DNA damage, free MMAF did not potentiate

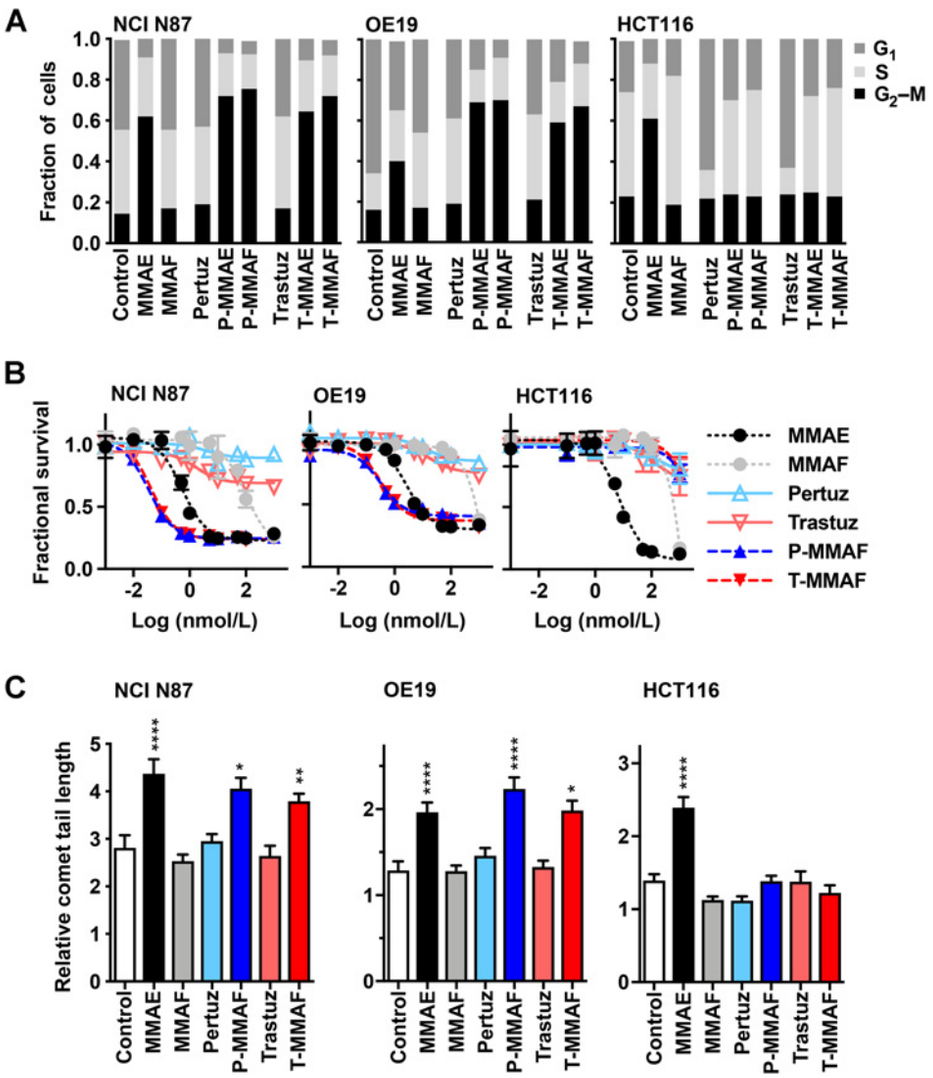

Figure 2.

MMAF cytotoxicity and radiosensitization require antibody conjugation. **A,** Cell-cycle distribution of drug-treated cells. NCI N87, OE19, and HCT116 cells treated with 2 nmol/L of free auristatin (MMAE or MMAF), anti-HER2 antibody (pertuzumab or trastuzumab), or ADC (P-MMAE, P-MMAF, T-MMAE, or T-MMAF) overnight, stained with propidium iodide, and analyzed by flow cytometry. **B,** Cytotoxicity of free drug, antibody, or ADC-treated cells. Cells exposed to a dose range of drug for 72 hours. Cell viability measured by Alamar Blue assay, normalized to control untreated cells, and plotted as mean fractional survival ± SD. **C,** IR-induced DNA damage. Cells treated with 1 nmol/L drug overnight, irradiated with 2 Gy, and DNA double-strand breaks measured by neutral comet assay. Comet tail lengths normalized to nonirradiated cells and plotted as mean relative comet tail length ± SEM. Statistical significances calculated using one-way ANOVA with Tukey multiple comparisons test (*, $P < 0.05$; **, $P < 0.01$; ****, $P < 0.0001$).

IR-mediated DNA damage. Importantly, P-MMAF and T-MMAF demonstrated HER2-restricted radiosensitization by significantly increasing IR-induced DNA damage to levels similar to free MMAE in HER2-expressing NCI N87 and OE19 cells but not HER2-negative HCT116 cells. Taken together, these findings establish the necessity of antibody conjugation for MMAF tumor kill and radiosensitization.

MMAF anti-HER2 antibody conjugates spatially target HER2-expressing tumors

Improving the therapeutic ratio of concurrent chemoradiotherapy can be achieved by selective systemic drug delivery to irradiated tumor targets while avoiding adjacent normal tissue. To test this, we advanced our ADC studies to murine tumor xenograft models differing in HER2 expression. First, we measured ADC drug delivery to tissue (**Fig. 3A**). Both P-MMAF and T-MMAF produced significantly higher drug levels in HER2-positive NCI N87 and OE19 tumors compared with HER2-negative HCT116 tumors. Moreover, tumor tissue was significantly enriched for MMAF compared with adjacent noncancerous muscle in mice with HER2-expressing tumors. Next, we tested MMAF's functional activity to block cells in G_2–M by measuring phosphorylation of Histone H3 at serine 10 (43). NCI N87 and OE19 tumors harvested from mice treated with P-MMAF or T-MMAF had prominent pS10 Histone H3 staining by IHC compared with control or antibody alone–treated mice at 24 hours (**Fig. 3B**). In NCI N87 tumors, P-MMAF and T-MMAF produced a 1.7- and 2.1-fold increase in pHistone H3 staining, respectively (**Fig. 3C**). In OE19 tumors, P-MMAF and T-MMAF produced a 6.1- and 3.5-fold increase in pHistone H3 staining, respectively. Importantly, HER2 specificity of ADC MMAF delivery was confirmed because HCT116 tumors treated with P-MMAF or T-MMAF showed no change in pHistone H3.

MMAF antibody conjugates reduced bystander toxicity

To synthesize our ADCs, auristatins were attached to antibody using MC-VC-PABC linkers (**Fig. 4A**). Upon receptor-mediated

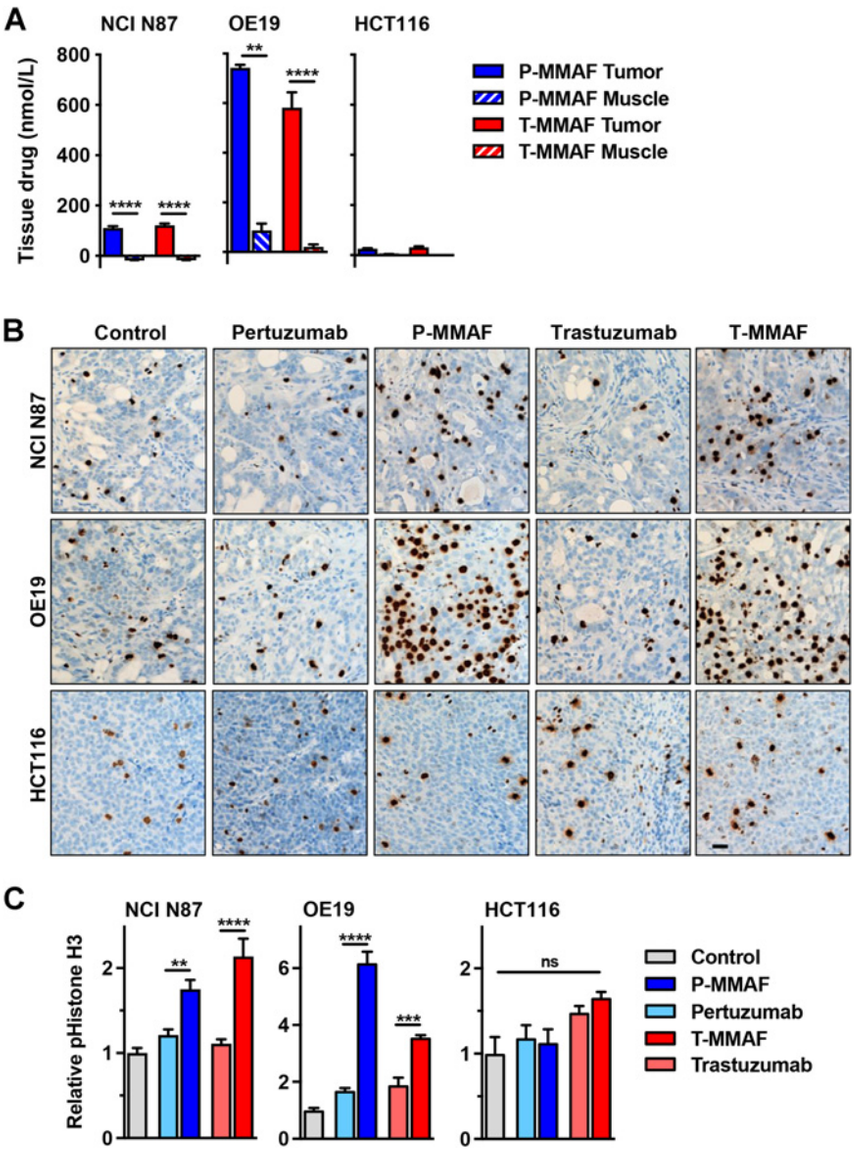

Figure 3.
MMAF anti-HER2 antibody conjugates restrict drug delivery to HER2 tumors. **A,** MMAF drug concentration in tumor and peritumoral normal tissue. NCI N87, OE19, and HCT116 tumor–bearing mice intravenously injected with 1 nmol of P-MMAF or T-MMAF. Tumor and adjacent normal tissue muscle harvested 24 hours later. Tissue drug concentrations quantitated by LC/MS-MS and plotted as mean ± SEM. **B** and **C,** Tumor-bearing mice intravenously injected with free antibody or MMAF antibody conjugate. Tumors harvested 24 hours later and stained for pS10 histone H3. **B,** Representative images of pS10 histone H3 staining. Black scale bar, 10 μm. **C,** Quantification of tumor pS10 histone H3. Data normalized to untreated control tumor tissue. Data plotted as mean relative tumor pS10 histone H3 ± SEM. Statistical significances were calculated using one-way ANOVA with Tukey multiple comparisons test (**, $P < 0.01$; ***, $P < 0.001$; ****, $P < 0.0001$). ns, not significant.

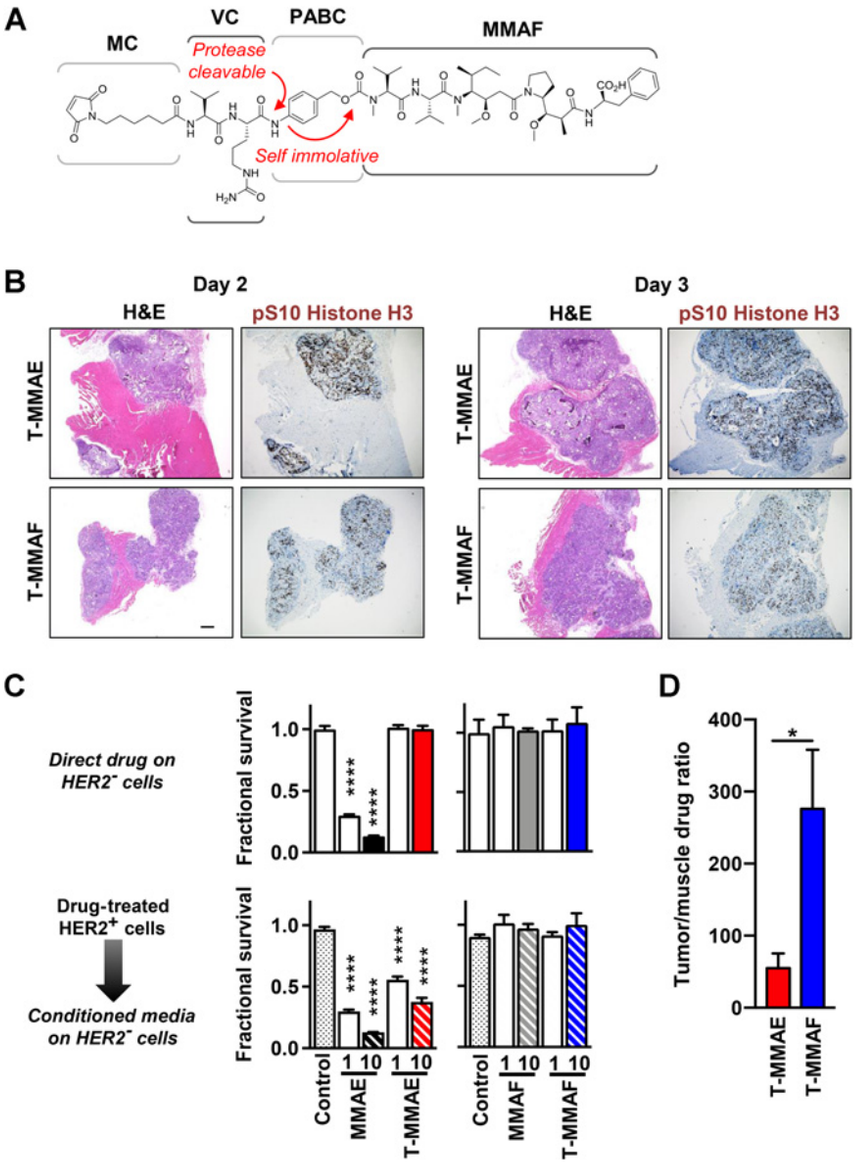

Figure 4.

MMAF antibody conjugates attenuated bystander toxicity. **A,** Schematic of maleimidocaproyl-valine citrulline-para amino benzyl carbamoyl (MC-VC-PABC) linker attached to MMAF. Cathepsin B cleavage at the citrulline amide releases free drug after self-immolative reaction of PABC. **B,** pS10 Histone H3 staining of tumor and peritumoral normal tissue muscle. NCI N87 tumor–bearing mice intravenously injected with 1 nmol of T-MMAE or T-MMAF and tissue harvested on days 2 and 3. Tissue sections stained with H&E and for pS10 histone H3. Black scale bar, 400 μm. **C,** Bystander cytotoxicity of auristatin antibody conjugates in cell culture. For direct effect, HER2-negative HCT116 cells were exposed to 1 or 10 nmol/L MMAE, T-MMAE, MMAF, or T-MMAF (top graphs), and cell viability measured by Alamar Blue. For bystander cytotoxicity, HER2-expressing NCI N87 cells were drug treated for 48 hours. Conditioned media were then transferred to HER2-negative HCT116 cells (bottom graphs). Cell viability measured by Alamar Blue assay, normalized to control untreated cells, and plotted as mean fractional survival ± SD. Statistical significances calculated using one-way ANOVA with Dunnett multiple comparisons test. **D,** ADC drug delivery in murine tissues. NCI N87 tumor–bearing mice intravenously injected with 1 nmol of T-MMAE or T-MMAF. Tumor and adjacent normal tissue muscle harvested 1 to 3 days later. Tissue drug concentrations quantitated by LC-MS/MS, and ratio of drug concentration in tumor and adjacent muscle tissues plotted as mean ± SEM (*, $P < 0.05$; ****, $P < 0.0001$).

internalization, the intervening valine–citrulline dipeptide is cleaved by endolysosomal cathepsin B to release drug after self-immolative loss of p-iminoquinone methide and CO_2. For MMAE, intracellular ADC uptake and subsequent drug release remove target restriction, and free MMAE can diffuse into adjacent cells and cause off-target toxicity. In contrast, ADC-released MMAF has attenuated cell permeability. Therefore, we investigated bystander differences of MMAE and MMAF warheads. T-MMAE or T-MMAF was intravenously injected into mice with NCI N87 tumors and tissue harvested. Sections containing both tumor and adjacent muscle were stained for pHistone H3 (**Fig. 4B**). By IHC, pHistone H3 staining was readily seen in HER2-rich tumor tissue but not peritumoral normal tissue. Interestingly, tumor tissue from T-MMAE–injected mice had more diffuse and pronounced pHistone H3 staining than T-MMAF, suggesting ADC-released MMAE was able to amplify mitotic arrest in neighboring tumor cells. To directly test this, we designed a cell culture model to quantitate bystander cytotoxicity (**Fig. 4C**; Supplementary Fig. S3). Free auristatins (MMAE or MMAF) or trastuzumab conjugate (T-MMAE or T-MMAF) were incubated with HER2-expressing NCI N87 cells. After 48 hours, conditioned media from these drug-treated cells were then transferred to HER2-negative cell HCT116, and cell viability was measured. As a control, a parallel set of HCT116 cells were directly exposed to free auristatins or trastuzumab conjugate. As expected, only free MMAE was directly cytotoxic to HER2-negative HCT116 cells (**Fig. 4C**). When conditioned media from drug-treated HER2-positive cells were transferred to HCT116 cells, conditioned media from T-MMAE group also became cytotoxic due to released MMAE. In contrast, conditioned media from MMAF- and T-MMAF–treated NCI N87 cells produced no off-target bystander toxicity in HCT116 cells. As a further control, the stability of our auristatin antibody conjugates

was confirmed using HCT116 cells as the source of conditioned media, proving T-MMAE intracellular uptake was necessary for bystander toxicity (Supplementary Fig. S3). Because IHC staining showed no appreciable pHistone H3 signal in peritumoral muscle, we measured tissue auristatin concentration by LC-MS to increase drug detection sensitivity. Mice with NCI N87 tumors were intra-

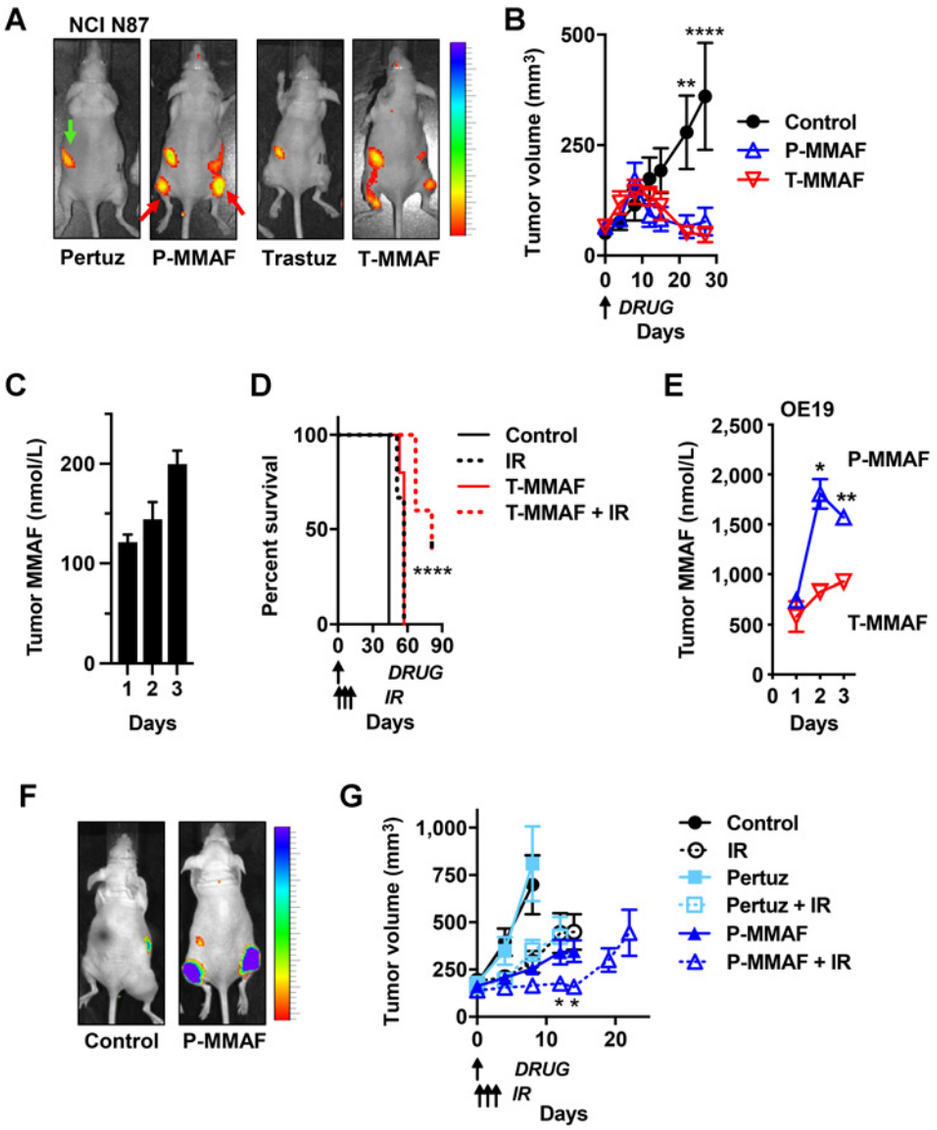

Figure 5.

MMAF anti-HER2 antibody conjugates improve tumor control with IR. **A,** Spatial localization of MMAF ADC in NCI N87 tumor xenografts grown in the thighs of mice (representative tumor locations indicated by red arrows in P-MMAF–injected mouse). Note that 1 nmol of unlabeled antibody (pertuzumab or trastuzumab) or Cy5-labeled P-MMAF or T-MMAF intravenously injected and whole mouse Cy5 fluorescence imaging 24 hours later. Gut autofluorescence indicated by green arrow. Scale bar on far right depicts dynamic range of Cy5 epifluorescence efficiency of 2.75×10^{-5} to 10×10^{-5}. **B,** Antitumor efficacy of MMAF ADC in NCI N87 tumor–bearing mice. Mice intravenously injected on day 0 with 1 nmol P-MMAF or T-MMAF. Tumors measured twice a week and plotted as mean tumor volume ± SEM. Statistical significances calculated using two-way ANOVA with Tukey multiple comparisons test. **C,** Kinetics of ADC tumor drug accumulation in NCI N87 tumors. Mice intravenously injected with 1 nmol T-MMAF on day 0. Tumors harvested on days 1, 2, and 3 after injection, and drug concentrations were quantitated and plotted as mean ± SEM. **D,** Antitumor efficacy of MMAF ADC with IR in NCI N87 tumors. Mice intravenously injected on day 0 with 0.5 nmol T-MMAF; 2.5 Gy given on days 1, 2, and 3. Mouse survival plotted and statistical significances calculated using log-rank (Mantel–Cox) test. **E,** Anti-HER2 antibody drug delivery in OE19 tumors. Mice intravenously injected on day 0 with 1 nmol P-MMAF or T-MMAF. Tumors harvested on days 1, 2, and 3 after injection, and drug concentrations measured and plotted as mean ± SEM. Statistical significances calculated using unpaired *t* test. **F,** Spatial localization of systemically delivered MMAF ADC in OE19 tumor xenografts. 1 nmol of P-MMAF i.v. injected and whole animal Cy5 fluorescence imaged 24 hours later. Scale bar on far right depicts dynamic range of Cy5 epifluorescence efficiency of 7×10^{-5} to 10×10^{-5}. **G,** Antitumor efficacy of MMAF ADC with IR in OE19 tumors. Mice intravenously injected on day 0 with 0.5 nmol pertuzumab or P-MMAF. IR given 2.5 Gy focally on days 1, 2, and 3. Tumors measured twice a week and plotted as mean tumor volume ± SEM. Statistical significances calculated using two-way ANOVA with Tukey multiple comparisons test (*, $P < 0.05$; **, $P < 0.01$; ****, $P < 0.0001$).

venously injected with T-MMAE and T-MMAF. Auristatin concentrations were quantitated in simultaneously harvested tumor and adjacent muscle (**Fig. 4D**). Importantly, T-MMAF–treated mice had a higher ratio of tumor to muscle drug delivery compared with T-MMAE, suggesting the less cell-permeable MMAF warhead resulted in greater target-specific ADC drug delivery.

MMAF anti-HER2 conjugates increase tumor xenograft control with IR

Because MMAF antibody conjugates had decreased bystander effect while maintaining HER2-targeted cell kill and radiosensitization, we tested the therapeutic potential of MMAF anti-HER2 antibody conjugates with IR. The first series of experiments used HER2-expressing NCI N87 tumor xenografts. Noninvasively tracking Cy5-labeled ADC demonstrated Cy5 fluorescence spatially localized to NCI N87 tumors but not HER2-negative HCT116 tumors (**Fig. 5A**; Supplementary Fig. S4). To evaluate intrinsic antitumor efficacy of P-MMAF and T-MMAF, tumor-bearing mice were treated with a single ADC injection of 1 nmol. Both P-MMAF and T-MAMF produced significant tumor regression (**Fig. 5B**). We terminated the experiment on day 60 at which time 3 of 5 mice treated with P-MMAF and 4 of 5 mice treated with T-MMAF showed no tumor regrowth. These results emphasize the inherent antitumor potency and efficacy of auristatin-based ADCs.

To optimally integrate MMAF antibody conjugates with IR, the temporal kinetics of ADC tumor drug delivery was assessed. A single intravenous injection of P-MMAF or T-MMAF resulted in an increased tumor fraction in G_2–M for 3 days as measured by pHistone H3 staining (Supplementary Fig. S5). Correlating with these histologic findings, a single injection of T-MMAF produced detectable tumor drug levels for 3 days (**Fig. 5C**). To evaluate ADC with IR, T-MMAF was dose decreased to a noncurative single 0.5 nmol/L injection. Because IR is clinically given over multiple days and ADC effect persisted for 3 days, tumors were treated with ADC followed by focal IR for 3 consecutive days. Although T-MMAF or IR monotherapies modestly increased survival, combining T-MMAF with IR significantly improved survival of NCI N87 tumor–bearing mice (**Fig. 5D**). To quantitate tumor growth statistics, we determined the number of days it took for tumors to reach 500 mm^3. For control, IR, T-MMAF alone, or T-MMAF + IR, it took 25, 39, 47, and 62 days respectively to reach 500 mm^3.

To confirm these findings, studies were validated in a second HER2-expressing tumor xenograft model, OE19. OE19 tumor drug delivery of MMAF antibody conjugates was measured (**Fig. 5E**). Consistent with the NCI N87 model, mice injected with P-MMAF and T-MMAF had detectable drug in tumors for 3 days. Interestingly for OE19 tumors, pertuzumab conjugation resulted in increased drug accumulation and pHistone H3 staining compared with trastuzumab (**Figs. 3C** and **5E**). Therefore, pertuzumab conjugates were advanced for testing with IR in OE19 tumor xenografts. Consistent with our prior results on MMAE peptide drug conjugates, MMAE conjugated to pertuzumab significantly delayed tumor growth (Supplementary Fig. S6; refs. 29, 30). Importantly, P-MMAF spatially localized to tumors by whole animal fluorescence imaging (**Fig. 5F**), and P-MMAF with IR significantly delayed tumor growth (**Fig. 5G**). Measuring time for tumors to reach 500 mm^3, we found it took 6, 12, 6, 12, 16, and 26 days for control, IR, pertuzumab, pertuzumab + IR, P-MMAF, and P-MMAF + IR groups, respectively. From a safety perspective, no adverse effect of combining ADC with IR on well-being was seen by mouse weight (Supplementary Fig. S7).

Discussion

Concurrent chemotherapy and radiotherapy remains the standard of care for nonmetastatic advanced cancers not amenable to surgical cure (1). Although IR techniques have improved to better conform IR dose to tumor and spare normal tissue, classical cytotoxic chemotherapies (cisplatin, taxanes, and 5-FU) remain the workhorse of combined treatment regimens with radiotherapy (2, 3). There are strong rationales for delivering systemic therapies with focal radiotherapy including: (i) Combined therapy can achieve tumor control at lower, safer, and more tolerable doses of each individual therapy compared with higher doses necessary as monotherapy. This is a clinically relevant issue because even though MMAF antibody conjugates have decreased drug permeability, these ADCs have side effects including thrombocytopenia and ocular toxicity (36). We showed that although dose-reduced T-MMAF did not produce long-term tumor regression alone, subtherapeutic doses of ADC with IR significantly improved tumor control (**Fig. 5B** and **D**). Therefore, lower dose of MMAF ADC with IR may decrease patient toxicities seen with monotherapy doses of MMAF. (ii) Concurrent chemoradiotherapy simultaneously attacks the known tumor but also potential subclinical metastatic disease. For locally advanced tumors, there is concern that undetectable cancer spread limits the efficacy of purely local therapies. Clinically, chemoradiotherapy is more effective when given concurrently as opposed to sequentially (9). However, chemotherapy and radiotherapy each induces side effects limiting patient tolerability of concurrent delivery. Therefore, targeted drug delivery scaffolds (i.e., ADCs) may facilitate treatment intensification with more potent cytotoxins given with radiotherapy to immediately attack the identifiable gross tumor and any metastatic spread. (iii) Drugs and IR kill tumors through different mechanisms, decreasing the emergence of therapy-resistant tumor clones. Despite ADCs having potent cytotoxic warheads, ADC resistance is documented (44). Therefore, in addition to the potential of ADC warhead radiosensitization, delivering ADCs with IR maximizes initial tumor kill by independent mechanisms and potentially offers improved tumor curability.

We have focused on testing trastuzumab and pertuzumab auristatin conjugates with IR since a HER2-targeted ADC is clinically approved (24). Importantly, HER2 is overexpressed in a proportion of tumor histologies treated with concurrent chemoradiotherapy, i.e., gastro-esophageal, non–small cell lung, and bladder cancers. Curiously, HER2 signaling has been implicated IR resistance. For this reason, clinical trials are evaluating HER2 inhibitors (i.e., trastuzumab and lapatinib) with radiotherapy (45). However, our radiosensitization approach fundamentally differs from HER2 pathway blockade. We have leveraged ADC technology so that HER2 serves as a molecular beacon to deliver highly cytotoxic and radiosensitizing auristatins. Such a HER2 radiosensitization strategy may maximize tumor kill because it circumvents resistance mediated by signaling pathway crosstalk (19, 20). Although not in solid cancer, combining brentuximab-vedotin with radiotherapy has shown promise in lymphoma (46). Another exciting potential is engaging the immune system. Immunooncology approaches are showing promise, and integrating IR is being actively pursued. Trastuzumab has been reported to induce antibody-dependent cell-mediated cytotoxicity (47). It is tantalizing to hypothesize there may be a role for ADC-based radiosensitization to engage antitumor immune responses.

ADC architecture is modular with three components: targeting antibody, warhead, and intervening linker. A major limitation of ADC has been identifying cell surface receptor targets differentially

expressed on tumors and normal tissue. Excitingly, there is continued progress on identifying cell surface receptors preferentially found on tumors that provide localizing antigen for unique antibodies (19, 20). Importantly, many of these antibodies are being developed for solid tumors routinely treated with chemoradiotherapy. Linker technologies attaching warhead to antibody are also being refined. We used the MC-VC-PABC linker to conjugate MMAF to anti-HER2 antibodies. An advantage of this linker is predictable release of free drug by cathepsin B within lysosomes. This allowed us to use LC/MS techniques to quantitate tissue drug accumulation. However, this linker is subject to retro-Michael reaction with premature release of drug into plasma (48). More stable linkers may reduce untimely drug release and resulting off-target toxicity. A complementary strategy to enhance safety is using warheads with decreased cell permeability as free drug. This was a primary motivation for us to synthesize MMAF ADCs. Interestingly, there is an MMAF ADC in clinical development targeting mutant EGFR brain tumors (49). Finally, other chemical classes of warheads are being developed to block critical cancer cell processes and may potentiate radiotherapy. For example, a topoisomerase I inhibitor has been attached to trastuzumab to target breast and gastro-esophageal HER2 tumors and could potentially radiosensitize (50). As the role of ADCs gains traction in cancer therapy, future clinical trials should consider including them in the upfront curative setting of locally advanced cancers treated in combination with radiotherapy in a biomarker-driven approach to concurrent chemoradiotherapy.

Disclosure of Potential Conflicts of Interest

E.E.W. Cohen is a consultant at Amgen, AstraZeneca, Bayer, BMS, Incyte, MSD, Merck, and EMD Sereno. A.M. Lowy is a consultant at Huya, reports receiving a commercial research grant from Syros, and has provided expert testimony for Rodney K. Norton/Hart Wagner. No potential conflicts of interest were disclosed by the other authors.

Authors' Contributions

Conception and design: D.V. Hingorani, E.E.W. Cohen, S.R. Adams, S.J. Advani
Development of methodology: D.V. Hingorani, M.F. Camargo, J. Aguilera, S.R. Adams
Acquisition of data (provided animals, acquired and managed patients, provided facilities, etc.): D.V. Hingorani, M.F. Camargo, J. Aguilera, S.M. Song, D. Pizzo, A.M. Lowy, S.R. Adams, S.J. Advani
Analysis and interpretation of data (e.g., statistical analysis, biostatistics, computational analysis): D.V. Hingorani, M.K. Doan, M.F. Camargo, E.E.W. Cohen, S.R. Adams, S.J. Advani
Writing, review, and/or revision of the manuscript: D.V. Hingorani, M.K. Doan, E.E.W. Cohen, A.M. Lowy, S.R. Adams, S.J. Advani
Administrative, technical, or material support (i.e., reporting or organizing data, constructing databases): M.F. Camargo, D.J. Scanderbeg, A.M. Lowy
Study supervision: S.J. Advani

Acknowledgments

The authors thank Evangeline Mose and Kersi Pestonjamasp for excellent technical assistance. This work was supported by grants from NIH/NCI [CA155620 (to A.M. Lowy), CA205765 (to S.J. Advani), CA219744 (to S.J. Advani), and CA215081 (to S.J. Advani)] and University of California Cancer Research Coordinating Committee [CRN-14-201501 (to S.J. Advani) and CRR-17-422691 (to S.J. Advani)]. UCSD Moores Cancer Center Comprehensive Biorepository and Microscopy Shared Facility were funded by NCI P30CA23100.

The costs of publication of this article were defrayed in part by the payment of page charges. This article must therefore be hereby marked *advertisement* in accordance with 18 U.S.C. Section 1734 solely to indicate this fact.

Received November 21, 2018; revised June 7, 2019; accepted September 30, 2019; published first October 9, 2019.

References

1. Moding EJ, Kastan MB, Kirsch DG. Strategies for optimizing the response of cancer and normal tissues to radiation. Nat Rev Drug Discov 2013;12:526–42.
2. Liauw SL, Connell PP, Weichselbaum RR. New paradigms and future challenges in radiation oncology: an update of biological targets and technology. Sci Transl Med 2013;5:173sr2.
3. Falls KC, Sharma RA, Lawrence YR, Amos RA, Advani SJ, Ahmed MM, et al. Radiation-drug combinations to improve clinical outcomes and reduce normal tissue toxicities: current challenges and new approaches: report of the symposium held at the 63rd annual meeting of the Radiation Research Society, 15–18 October 2017; Cancun, Mexico. Radiat Res 2018; 190:350–60.
4. Nigro ND, Vaitkevicius VK, Considine B. Combined therapy for cancer of the anal canal: a preliminary report. Dis Colon Rectum 1974;17:354–6.
5. Herskovic A, Martz K, Al-Sarraf M, Leichman L, Brindle J, Vaitkevicius V, et al. Combined chemotherapy and radiotherapy compared with radiotherapy alone in patients with cancer of the esophagus. N Engl J Med 1992;326:1593–8.
6. UK Co-ordinating Committee on Cancer Research. Epidermoid anal cancer: results from the UKCCCR randomised trial of radiotherapy alone versus radiotherapy, 5-fluorouracil, and mitomycin. UKCCCR Anal Cancer Trial Working Party. Lancet 1996;348:1049–54.
7. Al-Sarraf M, LeBlanc M, Giri PG, Fu KK, Cooper J, Vuong T, et al. Chemoradiotherapy versus radiotherapy in patients with advanced nasopharyngeal cancer: phase III randomized Intergroup study 0099. J Clin Oncol 1998;16: 1310–7.
8. Morris M, Eifel PJ, Lu J, Grigsby PW, Levenback C, Stevens RE, et al. Pelvic radiation with concurrent chemotherapy compared with pelvic and para-aortic radiation for high-risk cervical cancer. N Engl J Med 1999;340:1137–43.
9. Furuse K, Fukuoka M, Kawahara M, Nishikawa H, Takada Y, Kudoh S, et al. Phase III study of concurrent versus sequential thoracic radiotherapy in combination with mitomycin, vindesine, and cisplatin in unresectable stage III non–small-cell lung cancer. J Clin Oncol 1999;17:2692–9.
10. Macdonald JS, Smalley SR, Benedetti J, Hundahl SA, Estes NC, Stemmermann GN, et al. Chemoradiotherapy after surgery compared with surgery alone for adenocarcinoma of the stomach or gastroesophageal junction. N Engl J Med 2001;345:725–30.
11. Morris ZS, Harari PM. Interaction of radiation therapy with molecular targeted agents. J Clin Oncol 2014;32:2886–93.
12. Morgan MA, Parsels LA, Maybaum J, Lawrence TS. Improving the efficacy of chemoradiation with targeted agents. Cancer Discov 2014;4:280–91.
13. Kesari S, Advani SJ, Lawson JD, Kahle KT, Ng K, Carter B, et al. DNA damage response and repair: insights into strategies for radiation sensitization of gliomas. Future Oncol 2011;7:1335–46.
14. Bristow RG, Alexander B, Baumann M, Bratman SV, Brown JM, Camphausen K, et al. Combining precision radiotherapy with molecular targeting and immunomodulatory agents: a guideline by the American Society for Radiation Oncology. Lancet Oncol 2018;19:e240–51.
15. Lin SH, George TJ, Ben-Josef E, Bradley J, Choe KS, Edelman MJ, et al. Opportunities and challenges in the era of molecularly targeted agents and radiation therapy. J Natl Cancer Inst 2013;105:686–93.
16. Liu FF, Okunieff P, Bernhard EJ, Stone HB, Yoo S, Coleman CN, et al. Lessons learned from radiation oncology clinical trials. Clin Cancer Res 2013;19:6089–100.
17. Higgins GS, O'Cathail SM, Muschel RJ, McKenna WG. Drug radiotherapy combinations: review of previous failures and reasons for future optimism. Cancer Treat Rev 2015;41:105–13.
18. Sievers EL, Senter PD. Antibody-drug conjugates in cancer therapy. Annu Rev Med 2013;64:15–29.
19. Nagayama A, Ellisen LW, Chabner B, Bardia A. Antibody–drug conjugates for the treatment of solid tumors: clinical experience and latest developments. Target Oncol 2017;12:719–39.
20. Beck A, Goetsch L, Dumontet C, Corvaïa N. Strategies and challenges for the next generation of antibody–drug conjugates. Nat Rev Drug Discov 2017;16:315–37.

21. Younes A, Bartlett NL, Leonard JP, Kennedy DA, Lynch CM, Sievers EL, et al. Brentuximab vedotin (SGN-35) for relapsed CD30-positive lymphomas. N Engl J Med 2010;363:1812–21.
22. Okeley NM, Alley SC, Senter PD. Advancing antibody drug conjugation: from the laboratory to a clinically approved anticancer drug. Hematol Oncol Clin North Am 2014;28:13–25.
23. Girish S, Gupta M, Wang B, Lu D, Krop IE, Vogel CL, et al. Clinical pharmacology of trastuzumab emtansine (T-DM1): an antibody–drug conjugate in development for the treatment of HER2-positive cancer. Cancer Chemother Pharmacol 2012;69:1229–40.
24. Verma S, Miles D, Gianni L, Krop IE, Welslau M, Baselga J, et al. Trastuzumab emtansine for HER2-positive advanced breast cancer. N Engl J Med 2012;367:1783–91.
25. Kantarjian HM, DeAngelo DJ, Stelljes M, Liedtke M, Stock W, Gökbuget N, et al. Inotuzumab ozogamicin versus standard of care in relapsed or refractory acute lymphoblastic leukemia: final report and longterm survival followup from the randomized, phase 3 INOVATE study. Cancer 2019;125:2474–87.
26. Amadori S, Suciu S, Selleslag D, Aversa F, Gaidano G, Musso M, et al. Gemtuzumab ozogamicin versus best supportive care in older patients with newly diagnosed acute myeloid leukemia unsuitable for intensive chemotherapy: results of the randomized phase III EORTC-GIMEMA AML-19 trial. J Clin Oncol 2016;34:972–9.
27. Lambert JM, Berkenblit A. Antibody–drug conjugates for cancer treatment. Annu Rev Med 2018;69:191–207.
28. Palanca-Wessels MCA, Czuczman M, Salles G, Assouline S, Sehn LH, Flinn I, et al. Safety and activity of the anti-CD79B antibody–drug conjugate polatuzumab vedotin in relapsed or refractory B-cell non-Hodgkin lymphoma and chronic lymphocytic leukaemia: a phase 1 study. Lancet Oncol 2015;16:704–15.
29. Buckel L, Savariar EN, Crisp JL, Jones KA, Hicks AM, Scanderbeg DJ, et al. Tumor radiosensitization by monomethyl auristatin E: mechanism of action and targeted delivery. Cancer Res 2015;75:1376–87.
30. Adams SR, Yang HC, Savariar EN, Aguilera J, Crisp JL, Jones KA, et al. Anti-tubulin drugs conjugated to anti-ErbB antibodies selectively radiosensitize. Nat Commun 2016;7:13019.
31. Bourillon L, Bourgier C, Gaborit N, Garambois V, Llès E, Zampieri A, et al. An auristatinbased antibodydrug conjugate targeting HER3 enhances the radiation response in pancreatic cancer. Intl J Can 2019;145:1838–51.
32. Barok M, Joensuu H, Isola J. Trastuzumab emtansine: mechanisms of action and drug resistance. Breast Cancer Res 2014;16:209.
33. Tsui CK, Barfield RM, Fischer CR, Morgens DW, Li A, Smith BA, et al. Systematic identification of regulators of antibody-drug conjugate toxicity using CRISPR-Cas9 screens. bioRxiv 2019:557454. doi: 10.1101/557454.
34. Hamblett KJ, Jacob AP, Gurgel JL, Tometsko ME, Rock BM, Patel SK, et al. SLC46A3 is required to transport catabolites of noncleavable antibody maytansine conjugates from the lysosome to the cytoplasm. Cancer Res 2015;75:5329–40.
35. Doronina SO, Mendelsohn BA, Bovee TD, Cerveny CG, Alley SC, Meyer DL, et al. Enhanced activity of monomethylauristatin F through monoclonal antibody delivery: effects of linker technology on efficacy and toxicity. Bioconjug Chem 2006;17:114–24.
36. Masters JC, Nickens DJ, Xuan D, Shazer RL, Amantea M. Clinical toxicity of antibody drug conjugates: a meta-analysis of payloads. Invest New Drugs 2018:36:121–35.
37. Lyon RP, Meyer DL, Setter JR, Senter PD. Conjugation of anticancer drugs through endogenous monoclonal antibody cysteine residues. Methods Enzymol 2012;502:123–38.
38. Sun MMC, Beam KS, Cerveny CG, Hamblett KJ, Blackmore RS, Torgov MY, et al. Reduction— alkylation strategies for the modification of specific monoclonal antibody disulfides. Bioconjug Chem 2005;16:1282–90.
39. Doronina SO, Toki BE, Torgov MY, Mendelsohn BA, Cerveny CG, Chace DF, et al. Development of potent monoclonal antibody auristatin conjugates for cancer therapy. Nat Biotechnol 2003;21:778–84.
40. Sanderson RJ, Hering MA, James SF, Sun MMC, Doronina SO, Siadak AW, et al. In vivo drug-linker stability of an anti-CD30 dipeptide-linked auristatin immunoconjugate. Clin Cancer Res 2005;11:843–52.
41. Damen CWN, Chen W, Chakraborty AB, van Oosterhout M, Mazzeo JR, Gebler JC, et al. Electrospray ionization quadrupole ion-mobility time-of-flight mass spectrometry as a tool to distinguish the lot-to-lot heterogeneity in N-glycosylation profile of the therapeutic monoclonal antibody trastuzumab. J Am Soc Mass Spectrom 2009;20:2021–33.
42. Advani SJ, Camargo MF, Seguin L, Mielgo A, Anand S, Hicks AM, et al. Kinase-independent role for CRAF-driving tumour radioresistance via CHK2. Nat Commun 2015;6:8154.
43. Mielgo A, Seguin L, Huang M, Camargo MF, Anand S, Franovic A, et al. A MEK-independent role for CRAF in mitosis and tumor progression. Nat Med 2011;17:1641–5.
44. García-Alonso S, Ocaña A, Pandiella A. Resistance to antibody–drug conjugates. Cancer Res 2018;78:2159–65.
45. Mignot F, Ajgal Z, Xu H, Geraud A, Chen JY, Mégnin-Chanet F, et al. Concurrent administration of anti-HER2 therapy and radiotherapy: systematic review. Radiother Oncol 2017;124:190–9.
46. Montana W, Buck DA, Smith T. Near complete response in a patient with classical Hodgkin lymphoma treated with brentuximab vedotin concurrent with radiation therapy. Case Rep Oncol 2017;10:795–801.
47. Collins DM, O'Donovan N, McGowan PM, O'Sullivan F, Duffy MJ, Crown J. Trastuzumab induces antibody-dependent cell-mediated cytotoxicity (ADCC) in HER-2-non-amplified breast cancer cell lines. Ann Oncol 2012;23:1788–95.
48. Lyon RP, Setter JR, Bovee TD, Doronina SO, Hunter JH, Anderson ME, et al. Self-hydrolyzing maleimides improve the stability and pharmacological properties of antibody-drug conjugates. Nat Biotechnol 2014;32:1059–62.
49. van Den Bent M, Gan HK, Lassman AB, Kumthekar P, Merrell R, Butowski N, et al. Efficacy of depatuxizumab mafodotin (ABT-414) monotherapy in patients with EGFR-amplified, recurrent glioblastoma: results from a multi-center, international study. Cancer Chemother Pharmacol 2017;80:1209–17.
50. Doi T, Shitara K, Naito Y, Shimomura A, Fujiwara Y, Yonemori K, et al. Safety, pharmacokinetics, and antitumour activity of trastuzumab deruxtecan (DS-8201), a HER2-targeting antibody–drug conjugate, in patients with advanced breast and gastric or gastro-oesophageal tumours: a phase 1 dose-escalation study. Lancet Oncol 2017;18:1512–22.